Technical Report ARAED-TR-91022

FRACTURE AND YIELD STRENGTHS OF COMPOSITION B AND TNT AS A FUNCTION OF PROCESSING CONDITIONS AND COMPOSITION

D. A. Wiegand
J. Pinto

December 1991

US ARMY
ARMAMENT MUNITIONS
& CHEMICAL COMMAND
ARMAMENT RDE CENTER

U.S. ARMY ARMAMENT RESEARCH, DEVELOPMENT AND ENGINEERING CENTER

Armament Engineering Directorate

Picatinny Arsenal, New Jersey

The views, opinions, and/or findings contained in this report are those of the author(s) and should not be construed as an official Department of the Army position, policy, or decision, unless so designated by other documentation.

The citation in this report of the names of commercial firms or commercially available products or services does not constitute official endorsement by or approval of the U.S. Government.

Destroy this report when no longer needed by any method that will prevent disclosure of its contents or reconstruction of the document. Do not return to the originator.

REPORT DOCUMENTATION PAGE

Form Approved
OMB NO. 0704-0188

1. AGENCY USE ONLY *(Leave blank)*	2. REPORT DATE	3. REPORT TYPE AND DATES COVERED
	December 1991	

4. TITLE AND SUBTITLE
FRACTURE AND YIELD STRENGTHS OF COMPOSITION B AND TNT AS A FUNCTION OF PROCESSING CONDITIONS AND COMPOSITION

5. FUNDING NUMBERS

6. AUTHOR(S)
D. A. Wiegand and J. Pinto

7. PERFORMING ORGANIZATION NAME(S) AND ADDRESS(ES)
ARDEC, AED
Energetics and Warheads Division (SMCAR-AEE)
Picatinny Arsenal, NJ 07806-5000

8. PERFORMING ORGANIZATION REPORT NUMBER
Technical Report ARAED-TR-91022

9. SPONSORING/MONITORING AGENCY NAME(S) AND ADDRESS(ES)
ARDEC, IMD
STINFO Br (SMCAR-IMI-I)
Picatinny Arsenal, NJ 07806-5000

10. SPONSORING/MONITORING AGENCY REPORT NUMBER

11. SUPPLEMENTARY NOTES

12a. DISTRIBUTION/AVAILABILITY STATEMENT
Approved for public release, distribution is unlimited.

12b. DISTRIBUTION CODE

13. ABSTRACT *(Maximum 200 words)*

The uniaxial compressive strength and the yield strength as determined by confined triaxial compression (uniaxial strain) of Composition B were found to be increased by changes in processing conditions and composition. In addition, Young's modulus (slope of the linear portion of the stress versus strain curve) was also increased by the same changes. The uniaxial compressive strength and modulus were also found to depend on the position in the cast from which the samples were taken for some casts. The results to date suggest that these effects are due primarily to changes in porosity and further that the changes in porosity are due to changes in processing conditions. Therefore, significant increases in strength and modulus may be accomplished by changes in processing conditions. The differences in the strengths of Composition B and TNT are also considered.

14. SUBJECT TERMS

Porosity	Fracture strength	Yield strength	Young's modulus
Processing	Composition	Comp B	TNT
Composite	Explosive	Uniaxial compression	Triaxial compression
Poisson's ratio	RDX	Cracking	Cracks

15. NUMBER OF PAGES
53

16. PRICE CODE

17. SECURITY CLASSIFICATION OF REPORT	18. SECURITY CLASSIFICATION OF THIS PAGE	19. SECURITY CLASSIFICATION OF ABSTRACT	20. LIMITATION OF ABSTRACT
UNCLASSIFIED	UNCLASSIFIED	UNCLASSIFIED	SAR

ACKNOWLEDGMENTS

The authors are indebted to S. Nicolaides for active participation in the planning stages of this work and to J. Hershkowitz for suggesting the compositions of the modified forms of Composition B. The authors are also indebted to D. Georgevich for assistance with data taking and to M. Joyce, G. Ziegler, T H. Chen, and Y. Lanzerotti for helpful discussions. The authors wish to thank C. Ribaudo for material characterization, G. Ziegler for casting TNT and Comp B, J. Jenkins for the machining of samples, and F. Glanzel for radiographic work.

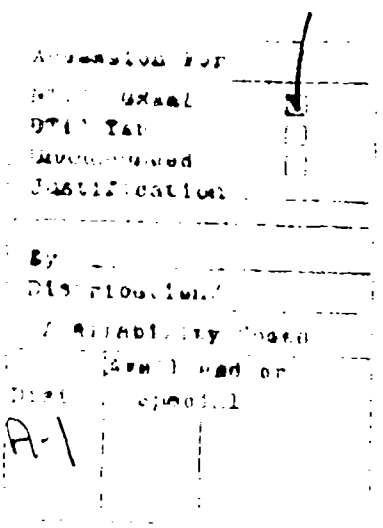

CONTENTS

TABLES

FIGURES

FIGURES (cont)

INTRODUCTION

This report is the third in a series concerned with mechanical failure of trinitrotoluene (TNT) and a composite of TNT and cyclotrimethylene trinitramine (RDX) (refs 1 and 2). This composite also contains 1% wax and is commonly known as Composition B (Comp B). TNT is the matrix material and both TNT and RDX are molecular organic polycrystalline solids. The first publication deals with the fracture properties (ref 1) and the second deals with the yield properties (ref 2) of the matrix and the composite as a function of temperature and strain rate. Significant differences in the strengths of the two materials were found. The fracture and yield strengths and Young's modulus are greater for the composite. In this publication two modifications of the composite are considered and the fracture and yield strengths are compared to those of the unmodified composite (Comp B) and to the matrix material (TNT). One of the modified composites (Comp B M1) was made without wax and with recrystallized TNT while the other modified composite (Comp B M2) was made with finer RDX particles (ref 3). Some changes in processing conditions were also made in attempts to obtain good quality casts.

The fracture properties of the two modified composites, the unmodified composite, and the matrix have been studied in uniaxial compression (ref 3). More limited studies were also made of the yield strengths of all four materials using triaxial confined compression as discussed previously (ref 2). The latter simulates the loading conditions which these materials experience during artillery launch and is also very similar to the loading conditions used in activators to study set-back sensitivity (refs 4 through 6). Young's modulus and Poisson's ratio were also obtained (ref 3). The terms Young's modulus or simply modulus and denoted by E are used rather loosely throughout when referring to the slope of the initial linear portion of the stress versus strain curve. It is desirable to distinguish between this slope and a true elastic modulus (constant). Similar considerations apply to Poisson's ratio. All results were obtained using the high strain rate as described previously, i.e., approximately 1.4 sec^{-1} and 4 sec^{-1} for the uniaxial and triaxial studies, respectively (refs 1 and 2). Failure occurred in a few milliseconds in all cases, which is the time frame of artillery launch. The temperatures were 23° and 35°C for the uniaxial and triaxial work, respectively.

Comp B is prepared by adding particulate RDX and wax to molten TNT and casting from the melt and TNT is prepared by casting from the melt. During the solidification and cooling processes, defects such as cracks, porosity, and larger voids and strain are introduced. These defects are important because they are thought to play critical roles in unwanted ignitions during gun launch and other uses. The ignition process also very often involves mechanical failure associated with the defect or defects. The mechanical properties such as the fracture and yield strengths and Young's modulus can be significantly affected by defects such as cracking and porosity

(refs 7 through 12). Defects introduced during casting can influence not only the mechanical strength and other properties and so influence the probability of unwanted ignitions in this way, but can also play a direct role in the mechanism or mechanisms of unwanted ignitions, e.g., by base gap closure not involving mechanical failure.

The goal of the program of which this work is a part has been to develop an understanding of mechanical failure in these materials and also as part of this program to develop the necessary understanding so as to be able to control the failure properties, e.g., how to develop materials of high strength. Complete stress versus strain curves to failure were taken in all cases and emphasis was placed on the compressive fracture strength, the yield strength, and for the work presented here, Young's modulus. Limited numbers of measurements were made which indicated trends. However, more extensive data are desirable to confirm the results and the interpretations given in this report. Finally, in no instance in these studies was any evidence of fast explosive reaction detected.

EXPERIMENTAL

The equipment and the data handling and reduction procedures are described in references 1 through 3. Samples were in the form of right circular cylinders, and two modes of compression were used. In one mode, the sample was subjected to uniaxial compression parallel to the cylinder axis (ref 1). In the other mode, the sample was confined in a tight fitting thick walled steel cylinder so that the radial strain was negligible during the applied axial compression (uniaxial strain) (ref 2). The results obtained from the confined cylinder (triaxial) mode of loading were corrected for the effects of friction between the steel cylinder wall and the explosive cylindrical surface, and graphite was used to minimize this friction (refs 3 and 13). All results presented were obtained using a medium strain rate, and typical curves of strain rate versus time are given in references 1 and 2. All of the uniaxial data presented were taken at 23°C, but in a few cases were corrected to 35°C by the use of a least squares straight line fit to the quantity in question plotted versus temperature. These corrections allowed direct comparison with the triaxial data which were taken at 35°C.

All samples used in these experiments were obtained from material cast in a split mold approximately 4 in. in diameter and 10 in. long (ref 3). Four explosives were studied and the compositions are given in table 1. TNT and Comp B are standard military explosives, while Comp B M1 and Comp B M2 are modifications of Comp B. Information regarding the RDX particle size distributions for the two varieties of RDX are given in table 2 along with the TNT melting points. The latter indicate that significant purification was probably not achieved by recrystallization.

In addition, there were differences in the casting procedures for the four explosives of table 1 (ref 3). Comp B and TNT as obtained from the manufacturing plants (Holston and Volunteer, respectively) were cast in the split mold. Some difficulties were experienced in obtaining "good" casts (i.e., sufficiently defect free casts), and these materials were cast several times before casts of only borderline acceptability for mechanical properties measurements were obtained. The split mold and riser were preheated on a steam table, the unfilled mold was wrapped in insulation, the Comp B was poured at 82°C, and a steam heated probe was inserted into the top to prevent rapid and localized solidification. TNT was cast with procedures similar to those for Comp B except that the pouring temperature was 76°C.

Comp B M1 and Comp B M2 were cast using procedures similar to those for Comp B and TNT. In addition, vacuum was applied to the melts of these materials for about 12 minutes, and the filled mold of Comp B M2 was vibrated for 12 sec. The pour temperature was 80°C for Comp B M1 and 92°C for Comp B M2. The higher temperature for the latter was necessary because of the higher viscosity which is due to the finer RDX. An acceptable quality cast of Comp B M2 was obtained on the first attempt, but several attempts were required to obtain a borderline quality cast of Comp B M1. The latter is to be expected because of the absence of the (supposedly) purified TNT. All casts were radiographed and acceptance or rejection was based on the quality as determined from the radiographs. The casting conditions are summarized in table 3.

The acceptable casts obtained from the split mold were cut into sections perpendicular to the cast axis. The sections were then further cut and machined into cylindrical samples with axes either parallel or perpendicular to the cast axis (ref 3). The samples were approximately 1.5 in. long with ends flat and parallel to ±0.001 in. The sample diameters were 0.7520 in. or slightly less and were uniform to 0.0005 in. All samples were radiographed after final machining, and samples with cracks and/or excessive porosity were discarded.

RESULTS

The results obtained using uniaxial compression are presented first and are followed by the results obtained by triaxial (radially confined) compression.

Uniaxial Compression

The four materials of table 1 have been studied in uniaxial compression, and typical stress versus strain curves for three of these materials are given in figure 1. The curves for Comp B M1 (not shown) are not significantly different from those of Comp B

M2. The curves for Comp B M1 and Comp B M2 are dependent on position in the cast and the curve for Comp B M2 was chosen to indicate an average difference between this material and Comp B and TNT. The curves of figure 1 indicate that the compressive strength, σ_m, and Young's modulus, E, as determined by the slope of the linear portion of the stress versus strain curve, increase on going from TNT to Comp B to Comp B M2 (and Comp B M1). The strains, ε_m, at the maximum compressive stresses do not show significant differences for the four materials. The results are summarized in table 4 where average values and standard deviations are given except for the σ_m and E values for Comp B M1 and Comp B M2. σ_m and E for these two materials are dependent on the position in the cast from which the sample was taken, and average values are given along with the range of observed values. The compressive strength of Comp B is almost a factor of two larger than that of TNT, while the average compressive strengths of Comp B M1 and Comp B M2 are about 30% greater than that of Comp B. In addition, the results of table 4 indicate that the average modulus, E, of Comp B is approximately 40% greater than the value for TNT, while the average moduli for Comp B M1 and Comp B M2 are about 35% greater than the average modulus for Comp B.

The compressive strengths and moduli for Comp B M1 and Comp B M2 are functions of the position in the cast. The compressive strengths of samples of Comp B M1 and Comp B M2 versus distance from a point near the top of the cast are given in figures 2 and 3.* The data of these two figures indicate that there is a significant increase in the compressive strength on going from the top to the bottom of the casts, and that this increase in greater for Comp B M1. In contrast, the compressive strengths of Comp B and TNT given in figures 4 and 5 as a function of position are independent of the position in the casts within the accuracy of the data. It must be noted, however, that only one cast of each of the materials of table 1 were prepared for this study. Therefore, the differences between Comp B, Comp B M1, and Comp B M2 can only be definitely related to these particular casts. More extensive measurements for Comp B and TNT indicate that the differences presented between these two materials are typical of the materials and not just the particular casts (ref 1 and 3).

The moduli of the samples of Comp B M1 and Comp B M2 are given as a function of position in the cast in figures 6 and 7. In figure 6 the moduli as obtained from both uniaxial and triaxial compression are given for Comp B M1. Triaxial data as a function of position was not obtained for Comp B M2. For figure 6, the moduli obtained from uniaxial measurement were corrected to 35°C from the temperature of measurement (23°C) for purposes of comparison. While there is considerable scatter in the data, the results presented in these two figures indicate that the moduli for these two materials

*Reference 14 is cited with figures 2 through 11 and 14.

are functions of the distance from the top of the cast. This statement can be made more conclusively for Comp B M2 than for Comp B M1. There is more uncertainty in the moduli as obtained from the triaxial measurements than for the uniaxial measurements because of the method of obtaining the moduli from the triaxial data (ref 2 and 3).

In figures 8 and 9 the moduli for Comp B and TNT are given as a function of position and as is the case for the compressive strengths, the moduli for these two materials are independent of the position in the cast. The data of these two figures and of figure 6 also indicate that there is agreement between the moduli as obtained from the triaxial measurements and the moduli obtained more directly from the uniaxial measurements.

Poisson's ratio for Comp B M1 as determined from triaxial measurements is given versus position in figure 6. Data were obtained only for the bottom part of the cast and the results are not extensive enough to determine if this quantity is a function of position. They are given here for completeness. In figure 10, Poisson's ratio is given versus position for Comp B and TNT and indicates that this quantity is not a function of position for these two materials.

If the uniaxial results for Comp B M1, Comp B M2, Comp B and TNT are replotted as compressive strength versus modulus (fig. 11), the results clearly indicate a correlation between the moduli and the compressive strengths. It appears that the correlation between the moduli and the compressive strength is better than the correlation between these two quantities and position. These matters are considered further in the discussion section below.

Throughout the course of the work reported here and in reference 1, the scatter in the data for the moduli is greater than the scatter in the data for the compressive strengths. If the scatter are predominantly due to variations in sample perfection, the opposite trend might be expected since the modulus is a volume average quantity while the compressive strength is dependent on the properties of cracks and other imperfections and therefore is very sensitive to localized disorder. However, it appears that the different noise levels in the two transducers used to measure displacement and load is an important reason for this difference in scatter in the data. The noise level in the linear voltage differential transformer (LVDT) used to determine displacement is comparable to the signal at the lower values of displacement and so strain, while the noise level in the load cell is considerably lower than the signal at the lower values of load. Thus, the slope of the load versus displacement curve and so the slope of the stress versus strain curve can be affected by the noise in the LVDT, especially near the origin. This noise will influence the modulus (slope) but not the compressive strength since the compressive strength is taken at the maximum of the stress versus strain curve and involves only the load cell and not the LVDT. In addition, deviations from parallelism and flatness of the end surfaces of the cylindrical samples will tend to effect the stress

versus strain curves primarily in the initial regions, i.e., near the origin because the stress concentrations which are so induced in the vicinity of the sample surfaces will cause high deformations at low applied stresses. Therefore, the slope of the stress versus strain curve and so the apparent modulus will be affected more than the compressive strength in these cases. It appears that the larger scatter in the modulus values is due to the noise in the LVDT with a possible contribution from nonideal conditions at the end surfaces of the samples.

Samples were also prepared with axes parallel and perpendicular to the cast axis for all four materials. However, sufficient numbers of samples were not available to determine within the scatter of data if the compressive strengths and the moduli were different for the two orientations. The compressive strengths of Comp B samples taken at a much lower strain rate were found to be dependent on position as observed here and also to be larger for samples with axes perpendicular to the cast axis (ref 15). Samples with axes parallel to the cast axis were also obtained with sample axes coincident with the cast axis and samples with axes part way between the cast axis and the cast surface (ref 3). However, as above, sufficient numbers of samples were not available to determine within the scatter of the data if the compressive strengths and the moduli were different for these two types of samples.

Triaxial Compression

For the triaxial, confined cylinder geometry measurements were made of the axial applied stress, σ_a, the radial stress on the sample due to the radial confinement imposed by the thick walled steel cylinder, σ_r, and the net axial strain, ε_a. Typical curves of the radial stress versus the axial stress for Comp B, Comp B M2, and TNT are given in figure 12. Data for Comp B M2 for this figure were chosen to emphasize the difference between this composite and Comp B. Curves for Comp B M1 tend to be similar to those of Comp B M2. An initial straight line part of each curve (not shown in fig. 12) is for the elastic region, and from the slope of this line, Poisson's ratio was obtained (ref 2 and 3). For further increases in the applied axial stress, yield and plastic flow occur, and the straight lines at the higher stresses are for this yield or plastic region for each material. The yield strengths, Y, are obtained from the intercepts of these straight lines with the σ_a axis and are indicated in figure 12 (refs 2 and 3). From these data, yield strengths of 10,700 psi for Comp B M2, 7,200 psi for Comp B, and 3,200 psi for TNT are obtained. It is clear that the yield strength of Comp B is significantly greater than the yield strength of TNT and that the yield strength of Comp B M2 (and also Comp B M1) is greater than the value for Comp B for the data chosen. Therefore, Y changes in the same direction as σ_m with composition and processing conditions.

The axial stress of figure 13, σ_a, is given versus the axial strain, ε_a, for triaxial loading for the three materials of figure 12. The straight lines indicate the initial slopes, and Young's modulus is obtained from this slope for each material (ref 3). However, it is important to note that this slope is determined by both Young's modulus and Poisson's ratio. Poisson's ratio was determined first from the data of figure 12. From these data (figs. 12 and 13), Young's modulus for Comp B M2 is greater than the modulus for Comp B, and the modulus for Comp B is greater than the value for TNT (table 5). When the axial stress is increased sufficiently, yield occurs; this is evident in the curves of figure 13 by decreases in the slopes. It is clear from the curves of these figures that TNT yields at a very significantly lower axial stress than Comp B.

Average values (table 5) are given for the yield strengths (Y), Young's moduli (E), and Poisson's ratio (ν), for TNT, Comp B, Comp B M1, and Comp B M2. Standard deviations are also given in many cases, but because of the wide spread in the values of the yield strengths and moduli for Comp B M1 and Comp B M2, ranges are given rather than standard deviations. The average yield strength of Comp B is more than twice the average yield strength of TNT. In addition, the average yield strengths of Comp B M1 and Comp B M2 are approximately 50% greater than the value for Comp B.

In comparing the values of Young's moduli in table 4 as obtained from the uniaxial measurements and the values of table 5 as obtained from the triaxial measurements, the differences in the temperatures of measurement must be considered (23°C versus 35°C). When this is done, the data of these two tables indicate excellent agreement for Comp B, Comp B M1, and TNT and reasonable agreement for Comp B M2. As noted above, E varies in the same direction as σ_m and also as Y with composition and processing conditions. The differences in Poisson's ratio for the four materials are close to the standard deviations and therefore may not be significant.

In figures 4 and 5, Y is given as a function of position in the cast from which the sample was taken for TNT and Comp B, and the results indicate that Y is independent of position within the accuracy of the data for Comp B and that Y may decrease slightly with distance from the top of the cast for TNT. Only very limited triaxial data were taken as a function of position for Comp B M1, and triaxial data were not obtained as a function of position for Comp B M2 because the available samples were used for other measurements. The limited triaxial yield strength data for Comp B M1 is not presented as a function of position but indicates that the yield strength decreases with increasing distance from the top of the cast. The yield strength of Comp B M1 therefore changes with position in the opposite direction to the compressive strength (fig. 2). This conclusion must be taken as tentative because of the limited number of triaxial measurements.

The yield strength versus the modulus for Comp B, Comp B M1, Comp B M2, and TNT is given in figure 14. The data indicate a correlation between the yield strength and the modulus which is similar to the correlation between the compressive strength and the modulus of figure 11. The data points for Comp B M2 considered separately agree with the general trend of yield strength versus modulus of this figure. However, if the data points for Comp B M1 are considered separately, there is very little trend but only a scatter of points about a mean which serves to give the general correlation of Y versus E. The same is true for the data points for Comp B and TNT. It is important to remember that the data for Comp B M2 are all for the same position. Therefore, the correlation is between Y and E and not between these two quantities and position.

DISCUSSION

In order to develop an understanding of the relative strengths of the four materials for which data were presented, it is necessary to consider the effects of inhomogeneities such as grain boundaries, cracks, porosity, and other microstructure in TNT plus RDX particles and wax in standard and modified Comp B. Discussions of TNT and standard Comp B are followed by a discussion of the modified versions of Comp B. The uniaxial (fracture) and triaxial (yield) results are considered separately.

Uniaxial Results and Fracture

Fracture Strength of TNT

It is well known that the grain size has a very significant effect on strength of polycrystalline metals, ceramics, and some other classes of materials (ref 16). The dependence of strength can be related to grain size through the Petch equation

$$\sigma_{st} = \sigma_1 + H/G^{1/2} \tag{1}$$

where σ_{st} is the stress at failure, σ_1 is related to the stress required for dislocation multiplication, G is the grain size, and H is a material constant (ref 17). When σ_1 is zero (i.e., for negligible dislocation multiplication before fracture) this reduces to

$$\sigma_{st} = H/G^{1/2} \tag{2}$$

which is of the same form as the Griffith criterion for fracture as given by

$$\sigma_T = (2E\gamma/c\pi)^{1/2} \tag{3}$$

when G = c, the crack half length. σ_T is the tensile fracture strength, E is Young's modulus (a true elastic constant), γ is the fracture surface energy, and c is the crack or flaw half length. The Petch equation for brittle materials such as ceramics has been interpreted in terms of cracks at grain boundaries so that c = G. However, the measured values of H (eq 2) were found in several cases to be larger than the values predicated by the Griffith approach for polycrystalline ceramics (ref 18). Reasons for this discrepency are discussed by Coble and Parikh (ref 18). The cracks at grain boundaries may be generated during cooling by thermoelastic anisotropic effects and/or elastic anisotropic effects (ref 16). Both TNT and RDX are anisotropic (ref 19 through 21). The cracks may also be generated by microplastic effects (i.e., dislocation pile-up at grain boundaries or twinning) or by the slow growth of subcritical cracks which is arrested at grain boundaries.

Observation of grain boundary sizes were not made for the samples used in this study. However, Lanzerotti et al. have made visual observations of the grain sizes for TNT samples and also have analyzed TNT fracture surface profiles (ref 22). From their analysis they have concluded that fracture has occurred primarily at grain boundaries for the conditions of their experiments (i.e., primarily tensile stress at very low strain rates). It is very plausible that relationships such as equations 1 or 2 apply to TNT. Since the yield strength is approximately a factor of two greater than the compressive fracture strength, significant dislocation motion resulting in plastic flow is not expected to occur before fracture (ref 1 and 3); therefore, equation 2 appears to be preferred over equation 1. It is also known that the crystallization of TNT from the melt is sensitive to the presence of other materials and surfaces which can act as nucleating agents (ref 23). The variation of TNT grain size with crystallization condition is probably responsible for variations in reported values of TNT strength. For example, the very low value of compressive strength (330 psi) given by Oliver for a strain rate of 10^{-3} for "pure" TNT as reported by Smith and Thorpe may be due to these effects (ref 24).

An estimate of the flaw size for the TNT samples used in this study can be made by using equation 3 with the compressive fracture strength, the relationship between compressive and tensile fracture strength, and the modulus reported previously (assuming that the modulus as determined from the slope of the stress versus strain curve is a true elastic modulus). The fracture surface energy is given in the literature for similar organic crystalline compounds. At the low strain rate, the compressive strength is 960 psi, the modulus is 0.25×10^6 psi, the ratio of compressive to tensile fracture strength is approximately eight (ref 1), and the fracture surface energy is close to 0.1 Joules/m^2 (ref 25). Use of these numbers in equation 3 yields a flaw size of about 0.4 mm which is in the range of grain sizes reported for TNT by Lanzerotti et al. (ref 22). It is reasonable to conclude as did Lanzerotti et al. that the grain size determines the flaw size and that fracture occurs at grain boundaries in TNT. The latter assumes that

the grain size in the samples used in this work is of the same order of magnitude as those used by Lanzerotti et al. As pointed out by Rice, the fracture surface energies of polycrystalline materials are often greater than the fracture surface energies of single crystals (ref 26). Since the fracture surface energy used in the above estimate of the flaw size is a single crystal value, the fracture surface energy appropriate to polycrystalline TNT may be larger. This would result in a larger flaw size. Evidence has been presented for slow crack growth before rapid crack propagation to fracture as described by the Griffith condition, equation 3 (ref 1). Therefore, slow crack growth may proceed until this growth is arrested at grain boundaries. The crack size associated with subsequent rapid crack growth will then be equal to the grain size as indicated above. The crack size before slow crack growth will then be considerably smaller than the estimate of 0.4 mm.

Fracture Strength of Comp B

It is important to note at the onset of this discussion that the fracture of Comp B must of necessity involve the propagation of cracks through the TNT matrix but not necessarily through the RDX particles. Because the RDX particles are embedded in the TNT matrix, cracks may propagate through them, around them, or both. Therefore, in applying a Griffith type criterion for the conditions for rapid crack propagation, consideration must be given to the actual crack path and the effective values of the modulus and surface energy appropriate to that path. Therefore, the strength of the composite Comp B is determined in part by the crack path which influences the effective γ and the effective modulus.

The crack size in Comp B could be determined by the TNT grain size for TNT and/or by the RDX particle size or by other considerations. Cracks can be generated at the TNT/RDX interfaces because of differences in the thermal expansion coefficients and elastic constants. The thermal expansion coefficients of Comp B with and without wax (Comp B-3) are greater than the average values for TNT (ref 27), indicating that the average thermal expansion coefficient of RDX is greater than the average value of TNT. In addition, Young's modulus for Comp B is greater than the value for TNT, indicating that the average modulus of TNT, indicating that the average modulus of RDX is greater than the average modulus of TNT. Both of these effects will cause discontinuities, stress and strain concentrations, and tend to cause cracking at the RDX/TNT interfaces in Comp B. For these reasons the crack length may be determined by the RDX particle size.

The flaw size for rapid growth to fracture in Comp B has been estimated by the same method as used above for TNT and found to be about 0.2 mm. The fracture surface energy was taken as 0.1 Joules/m^2 (ref 25). This fracture surface energy and the estimated flaw size may be large if a significant amount of the fracture is between RDX particles and TNT as suggested by Lanzerotti et al. (ref 22). This flaw size is close

to the geometric mean particle size for class 1 RDX (table 2) (ref 22). If slow crack growth before fracture occurs primarily within the RDX particles, it may be arrested at the RDX/TNT interface. In this case the flaw (crack) size for rapid growth to fracture would be close to the RDX particle size. However, if slow crack growth occurs primarily in the TNT and is arrested at the RDX/TNT interface, the flaw size would be close to the geometric mean distance between RDX particles which in Comp B is significantly less than the RDX geometric mean particle size. The question of the relationship of the flaw size and so the strength to the RDX particle size is considered further below.

Costain and Motto report values of the compressive strength for Comp B-3 which are approximately the same as their values for Comp B at 23°, 52°, and 71°C for a low strain rate (ref 27). At lower temperatures (-40° and -62°C) the compressive strengths for Comp B-3 are considerably greater than the values for Comp B. In addition, the tensile strengths given by Costain and Motto for Comp B are mostly equal to or greater than the values for Comp B-3. Comp B-3 is made with class 6 RDX which has particle sizes considerably smaller than the values for class 1 RDX which is used in Comp B (ref 28). If the crack size is determined by the RDX particle size because of cracking between the RDX and TNT, then the fracture strength of Comp B-3 should be greater than the fracture strength of Comp B because of this difference in RDX particle sizes. These results of Costain and Motto (except for the compressive strengths at -40° and -62°C) suggest that in their samples the critical crack lengths in Comp B and Comp B-3 were not determined by the RDX particle sizes.

Comp B contains wax while Comp B-3 does not. Therefore, in a comparison of the results for these two materials, the effects of wax must also be considered. One effect of wax in Comp B is to reduce porosity, but for the densities given by Costain and Motto, the estimated porosity corrections to their compressive strengths for Comp B and Comp B-3 are negligible for this discussion. The effects of wax on the TNT grain size is unknown to the authors. In addition, the dependency of the crack path on the presence and distribution of wax must be considered in comparing strengths of these two forms of Comp B. The results of Costain and Motto suggest but do not establish that the critical length is not related to RDX particle size because of the unknown role of wax. It is assumed for this discussion that the processing conditions for the Comp B and Comp B-3 used by Costain and Motto were identical.

Similar considerations apply to the three forms of Comp B discussed here. Comp B M2 contains class 7 RDX while Comp B and Comp B M1 contain class 1 RDX (table 1). The RDX particle size of class 7 is significantly less than the particle size of class 1 (table 2). If there were no other significant differences between these three composites, the compressive strength of Comp B M2 should be greater than the strength of the other two as predicted by equation 3 if the flaw half lengths, c, were determined by RDX particle size considerations. The results indicate that this is not the case (table 4). However, Comp B and Comp B M2 contain wax while Comp B M1 does

not. All of the above comments regarding the effects of wax must be considered here also. In particular, Comp B M2 contains a smaller RDX particle size distribution than Comp B but does contain wax. If there were no other differences between these two composites, the effect of changing only the RDX particle size could be determined. However, there are differences in processing conditions for these two composites (and Comp B M1, see table 3) which are discussed below in another subsection.

The crack length in Comp B could also be determined by the TNT grain size. The TNT grain size for TNT in Comp B has been found to be considerably smaller than the grain size of TNT alone (ref 29). There should be a significant increase in the Comp B strength over TNT due to this effect alone if the flaw length is determined by the TNT grain size in the TNT of Comp B (eq 2). The strength of Comp B will also be determined by the second phase particle effect previously discussed and the modulus. Both of these factors will contribute to a higher strength for Comp B relative to TNT.

It is also necessary for Comp B to consider the conditions under which crack propagation occurs (i.e., the crack path as noted above). Calculations and experiments indicate that when a propagating crack approaches a discontinuity in elastic modulus such as the difference between RDX and TNT, the crack will be attracted to the regions of highest tensile stress concentration (ref 30). For a spherical particle in an isotropic medium in tension and for $E_{particle}$ greater than E_{medium}, the tensile stress will be greater at the poles through which the tensile axis passes and the stress will be compressive at the equator (ref 30). Therefore, a crack propagating in a plane perpendicular to the tensile axis in the medium will be deflected toward the poles and around the particle. However, if the stress field of the crack breaks the interfacial bond between the particle and the medium, the particle will appear as a pseudo-void with E_{void} less than E_{medium} and the crack will be attracted to the equator rather than being deflected around the particle (ref 30). In this case the crack may propagate through the particle or be arrested at the particle medium interface. In either case, additional energy is expended relative to the case without the particle so there will be an increase in strength, but the greater increase will result from breaking the interfacial bond. Additional energy may also be expanded by plastic deformation of the particle, leading to an even greater increase in strength (ref 30). The increase in strength with increase in energy dissipation by the crack can be understood in terms of the Griffith criterion for fracture (eq 3) by an increase in the effective γ. This will also increase H in equations 1 and 2. The actual path of the crack in the vicinity of a particle depends on the particle shape (ref 30), the interfacial bond strength (ref 30), the particle surface texture (refs 31 and 32) (this influences interfacial bond strength), and the strain rate (refs 32 and 33). The actual crack path determines the energy dissipated and the strength. The effect of

introducing particles of a second phase with $E_{particle} > E_{medium}$ increased the strength, e.g., Ni and Al in glass (ref 20) and rock in mortar to produce concrete (ref 33). The magnitude of the increase in strength is dependent on several parameters. It is important to note that the increased strength due to second phase particles is relative to the medium without particles.

Actual crack patterns have been observed in Comp B recovered after shell firing and Comp B fractured in the laboratory (ref 24). The strain rate for the former is not given but was most probably of the order of 1.0 sec^{-1} and for the latter the strain rate was 4.0×10^{3} sec^{1}. In both cases many crack paths were found to pass through RDX particles; therefore, the condition for increased strength due to RDX particles was met. By use of a lower strain rate, Lanzerotti et al. have concluded that the fracture occurs primarily between RDX and TNT in Comp B (ref 22). If an interfacial bond is broken during this low rate fracture, the strength should be influenced by this breaking. A similar dependence of crack path on strain rate was observed for concrete and the strength is larger at the higher rate (refs 32 and 33). The difference in crack paths and the larger strengths at the higher rate in concrete is attributed in part to cracks following shorter paths and so passing through regions of higher resistance (i.e., through aggregate particles at the high rate) because energy is deposited at a much higher rate. The difference in crack path and resultant difference in strength is probably not the major reason for the dependence on strain rate found for Comp B, because the two strain rates used (ref 1) are closer to the values used by Smith and Thorpe (ref 24). In the Smith and Thorpe work, the crack paths were found to pass through the RDX particles at both rates. The low strain rate used in the reported work (ref 1) is significantly greater than the rate used in the experiments of Lanzerotti et al. The strain rate dependence of the compressive strength was associated with slow crack growth (ref 1). As is the case with TNT, the flaw size before slow crack growth must be smaller than the flaw size (eq 3) for rapid crack growth to fracture.

In summary, the higher fracture strength of Comp B relative to TNT is probably due to the effects of RDX particles on the crack path. Differences in the TNT grain sizes may also play a role. In addition, the results to date suggest that the critical crack length is not related to the RDX particle size, but the separate effects of this particle size, wax, and processing conditions have not been determined.

Relative Fracture Strengths of the Composites

The reasons for the higher compressive strengths of Comp B M1 and Comp B M2 relative to Comp B are addressed in this subsection. Many factors can influence the fracture strength of brittle solids including porosity, microcracking, the modulus, and the surface energy. Since there appears to be a correlation between the modulus and

the compressive strength, it is also of interest to consider factors which can influence the modulus. These include porosity (ref 10) and microcracking (ref 9). Because these can have a direct effect on both the strength and the modulus, they are considered in some detail. This discussion is followed by considerations of other factors which can influence the strength.

The apparent linear relationship between the compressive strength, σ_m, and the modulus, E, for the three composites (fig. 11) indicates that both are approximately the same function of one or more variables so that the ratio σ_m/E is constant as these variables change. A discussion of porosity as the dominant variable is followed by a consideration of microcracking. The porosity, P, is taken as the fractional deviation of the measured density, ρ_m, from the maximum theoretical or ideal density, ρ_{TMD}, i.e.,

$$P = (\rho_{TMD} - \rho_m)/\rho_{TMD} = 1 - \rho_m/\rho_{TMD} \qquad (4)$$

The ρ_m were determined by measuring the weight and volume of each sample. Because the samples were precision machined, this method of determining density should give adequate accuracy and precision. The densities of almost all samples used in these studies were measured in this way but unfortunately the lengths were in some cases not determined with the necessary precision. In addition, the densities of the samples of Comp B M1 and Comp B M2 which were used for measurements of the compressive strength as a function of position were not measured. For these reasons, the densities and the porosities are not available for some of the samples of interest. The importance of the densities was not anticipated at the time that the measurements were made. The density data were taken only to provide some limited characterization of the samples.

The densities of the Comp B samples used in this work were found to be higher than the densities of Comp B given by some other workers. The average density of the samples of Comp B used here is 1.695 ± 0.004 g/cm and the available densities of the samples of Comp B M1 and Comp B M2 are somewhat higher. The uncertainty in this density is the standard deviation of the measured values. This density for Comp B is typical of the values obtained for whole casts using the casting techniques given in the experimental section and measuring weight and volume (ref 34). In contrast, Croom et al. recently determined the density of smaller samples of Comp B taken from a cast out of the same mold as used here and with similar but not identical processing conditions (ref 35). An immerson technique was used, and the value 1.617 ± 0.042 g/cm^3 reported. The difference between this latter value and the value given above may be associated with local density fluctuations and the small size of the samples measured by Croom et al. The density of Comp B obtained from a larger mold from a production

plant was also measured recently and found to be in the range 1.59 to 1.65 ± 0.02 g/cm^3 (ref 36). In this case the density increased from top to bottom of the cast. All densities in both of these cases are significantly less than the values obtained in this work. However, the samples of all four materials used in this study are expected to have higher densities than those generally reported because casts and samples having significant porosities and/or cracking as detected by x-ray radiography were discarded. As noted in the experimental section, some materials were cast several times before casts containing negligible porosity and/or cracking were obtained. In addition, individual samples were radiographed after machining and discarded if cracking was observable. These considerations may account for the higher densities found here as compared to the densities reported by some others.

In addition to small uncertainties in the measured densities, there are uncertainties in the maximum theoretical densities of the samples of the composites Comp B, Comp B M1, and Comp B M2 because of uncertainties in the compositions. Both uncertainties contribute to the uncertainties in the porosities. The compositions given in table 1 were not measured (with exception of the percentages of HMX). The composition of Comp B given in the table is the nominal composition and the extremes of densities allowed by the specifications result in an uncertainty in the porosity of about ±11%. The compositions of Comp B M1 and Comp B M2 are those of the melt. It is reasonable to conclude that there are similar uncertainties in the porosities of these two forms of Comp B due to this effect. In addition, it is necessary to consider the possibility of gradients in composition and porosity. Gradients in composition were observed (refs 35 and 36). For the larger casts, the gradients are not large enough to produce gradients in ρ_{TMD} (ref 36), but for the smaller casts obtained from the same mold and using casting procedures similar to those used in this study, the gradients are sufficient to result in significant gradients in ρ_{TMD} (ref 35). Because the compositions of the casts and samples were not measured, there is then significant uncertainty in the maximum theoretical densities. For this reason some emphasis is placed on the expected relationship between the compressive strength and Young's modulus when porosity is the controlling factor for both. However, results as a function of porosity are also presented. In estimating the porosities, the following densities were used in the calculations of the ρ_{TMD}: RDX--1.816 gm/cm^3, HMX--1.900 gm/cm^3, TNT--1.654 gm/cm^3, and wax--0.894 gm/cm^3. The wax density was measured by immersion of Petrolite (ES-670), the wax used in Comp B M2. The same wax density was used for Comp B although the type of wax in the Comp B from which the samples were made is unknown.

Because porosity can decrease the load bearing surface area and/or lead to stress concentrations, the local stress can be increased relative to the applied stress as porosity increases. The applied stress for failure (e.g., fracture) decreases with increasing porosity if the stress for failure does not change. Knudsen calculated the applied

tensile stress for failure as a function of porosity for one particular pore structure and has found that his results can be expressed as

$$\sigma_m = \sigma_o e^{-b_\sigma P} \tag{5}$$

where σ_o is the zero porosity failure stress and b_σ is a constant (ref 8). However, this type of equation was found to describe the experimental relationship between fracture strength and porosity for many brittle materials in tension and compression (ref 26).

Because of the increase in the local stress with increased porosity at constant applied stress, there is an increase in strain and so a decrease in the apparent elastic modulus. More recently Wang has calculated the apparent modulus for the same pore structure as used by Knudsen as a function of porosity and has found that his calculations can be expressed by

$$E = E_o e^{-b_E P - cP^2} \tag{6}$$

where E_o is the zero porosity modulus and b_E and c are constants (ref 10). Many materials can be described by this relationship. The equations for σ_m and E differ because the averaging processes for the stress and the modulus are different.

While these two equations are strictly only valid for the pore structure used by Knudsen and Wang and only for applied tensile stresses, they have more general applicability (ref 26). It is reasonable to apply them to Comp B in compression although the pore geometry is unknown. By combining equations 5 and 6

$$\sigma_m = E\sigma_o/E_o e^{-(b_\sigma - b_E)P} \tag{7}$$

$$\approx E\sigma_o/E_o(1 - (b_\sigma - b_E)P) \tag{8}$$

for

$$(b_\sigma - b_E)P << 1 \tag{9}$$

where the quadratic term was omitted from the expression for E. This omission and equation 9 are valid for sufficiently small values of P. Equations 7 and 8 predict a linear relationship between σ_m and E for sufficiently small values of porosity as found here. The observed relationship as shown in figure 11 is approximately linear in agreement with this model of porosity, and the hypothesis that the relationship between strength

and the modulus is determined by porosity. TNT data are included in figure 11 for completeness and fall along an extrapolation of the line through the Comp B, Comp B M1, and Comp B M2 results.

As noted above, density data are not available for the samples of Comp B M1 and Comp B M2 for which the compressive strengths were measured. However, densities are available for some of the samples of these two materials which were used for triaxial measurements. These samples were from positions near the bottom of the cast. The logarithms of the compressive strengths and the moduli from these positions are plotted versus porosity as determined from the triaxial samples and combined with data for Comp B in figures 15 and 16. Straight lines were fitted to the points (without TNT) as predicted by equations 5 and 6 to give values of $b_\sigma = 46$ and $b_E = 50$. These values are much larger than predicted by the calculations of Knudsen and Wang in tension and observed for other materials. Values of b_σ in the range 2.2 to 15 have been reported (ref 37). However, large values of b_σ have been observed in compression (ref 38). The large value of b_E is also not in agreement with the results of others (ref 39). These values of b_σ and b_E do, however, support the approximation of equation 9. From these same figures it is found that $\sigma_o = 9{,}100$ psi and $E_o = 1.8 \times 10^6$ psi. These indicate that the zero porosity strengths and moduli can be significantly greater than the values with porosity. Therefore, porosity may be the reason for some of the discrepancies between the moduli found in this work and the values reported by others (refs 1 and 2). Significant increases in strength and modulus can be attained by reducing porosity by, for example, modifying processing conditions (see below).

From equation 8 the slope of the σ_m versus E curve at zero porosity is σ_o/E_o and has the value of 0.50×10^{-2} if the above σ_o and E_o are used. From figure 11 this slope is 0.59×10^{-2}. This is very good agreement when consideration is given to the uncertainties in the slopes of figures 11, 15, and 16. This agreement also lends support to the porosities used in figures 15 and 16. If the TNT data are included in the determination of σ_o and E_o and the zero porosity slope of σ_m versus E, the agreement between the two methods of obtaining σ_o/E_o is also good. The data indicate $b_\sigma < b_E$ in agreement with the calculations of Knudsen and Wang. This also indicates that σ_m should decrease more rapidly with increasing P than E. There is too much scatter in the data of figure 11 to determine if this is, in fact, the case.

As noted above, the straight line which was fitted to the data points for the Comp B's on the graph of σ_m versus E also passes through the TNT points plotted on the same graph (fig. 11). Straight lines were also fitted to the data points of figures 15 and 16 including the data points for TNT. The density of the TNT samples used in this work is 1.590 ± 0.007 g/cm^3 and is typical of values obtained for whole casts using the

casting techniques given in the experimental section and measuring weight and volume (ref 34). TNT has the largest porosity and in this case the values of b_σ, b_ε, σ_o, and E_o are all less than the values from the data without TNT (figs. 15 and 16). If this analysis is meaningful, porosity must be the dominant factor in determining the differences between TNT and Comp B. For TNT to have the same E_c as the Comp B, the modulus of RDX must be close to the modulus of TNT since Comp B contains approximately 60% RDX. Measurements of the moduli of TNT and RDX without porosity are necessary to resolve this matter. For the compressive fracture strengths of TNT and Comp B to be primarily determined by porosity and to have the same values of σ_o, it seems necessary that the fracture processes in Comp B be largely confined to the TNT of Comp B and further that the factors which determine strength of the TNT such as the grain size be about the same for TNT alone and for the TNT in Comp B. As discussed above in another subsection, the latter seems unlikely. In addition, the porosity must be distributed in the TNT and RDX of Comp B so that the porosity of the Comp B is the same as the porosity of the TNT in the Comp B. This would be very fortuitous. For all of these reasons it is, therefore, tentatively concluded that porosity is not the major factor determining the differences in the compressive fracture strengths and the elastic moduli of TNT and Comp B.

The results as presented in figures 11, 15, and 16 indicate that the differences in the compressive fracture strengths and the moduli of Comp B, Comp B M1, and Comp B M2 are primarily due to porosity. These results and the above discussion further indicate that the gradients of strengths and moduli as a function of position in the cast for Comp B M1 and Comp B M2 as shown in figures 2, 3, 6, and 7 are also primarily due to gradients of porosity. The lack of these gradients for Comp B and TNT indicate uniform casts (figs. 4, 5, 8, and 9). The differences in the porosities of the casts of Comp B, Comp B M1, and Comp B M2 can be attributed to differences in the processing conditions. A vacuum was applied to the melts of Comp B M1 and Comp B M2 for 12 min but not to the melt of Comp B (or TNT). This treatment is expected to decrease the porosities of the former relative to the latter in agreement with observations because of the removal of trapped gas. In addition, the filled mold of Comp B M2 was vibrated for 12 sec while the filled molds of Comp B and Comp B M1 (and TNT) did not receive this treatment. The porosities of Comp B M2 were found to be lower than the porosities of the other two as expected from the difference in treatments. Therefore, the relative porosities and compressive fracture strengths and moduli of Comp B, Comp B M1, and Comp B M2 can be attributed to these differences in processing conditions (table 3). However, it is not clear why these differences in processing resulted in gradients for Comp B M1 and Comp B M2 but not for Comp B and TNT. Vibration of the filled mold of Comp B M2 combined with the higher pour temperature could result in trapped gasses rising toward the top and inducing a gradient of porosity, but the differences in processing conditions between Comp B and Comp B M1 do not account for their differences in gradients. As noted above, a gradient of density was observed recently for a larger cast of Comp B (ref 36).

Before concluding this discussion of porosity, it is useful to consider factors which may influence σ_o, the zero porosity compressive strength. As indicated by equations 1 and 2 and the associated discussion, the strength is related to a dimension G which in polycrystalline materials is often the grain size. In composite materials such as Comp B this dimensions could be the RDX particle size, but as discussed above, a consideration of the results of Costain and Motto for Comp B and Comp B-3 and consideration of the results for Comp B, Comp B M1, and Comp B M2 presented here suggest that this is not the case. While Comp B and Comp B M1 were made with class 1 (course) RDX, Comp B M2 was made with class 7 (fine) RDX. If the geometric mean RDX particle sizes are taken as the values of G in equation 2, the ratio of the compressive strengths corresponding to these two values of G is 1.67 when all other factors are the same. On this basis the zero porosity compressive strength of Comp B M2 should be 1.67 times the zero porosity values for Comp B and Comp B M1. The data of figure 11 and the attendant discussion of the applicability of equation 7 indicate that the zero porosity compressive strengths of all three forms of Comp B considered here are close in value. Therefore, the σ_o's cannot be sensitive to the RDX particle sizes and so the G's of equations 1 and 2 cannot be related directly to the RDX particle sizes for these materials. The G's may be determined primarily by the TNT grain size.

Comp B and Comp B M2 contain military grade TNT and wax while Comp B M1 contains recrystallized TNT and does not contain wax. The similarities of the zero porosity compressive strengths indicate that these differences also do not significantly affect the length parameter G which may be taken as a measure of the crack length. The results further indicate that these differences do not affect the crack path and therefore do not effect surface energy.

As pointed out above, microcracking is thought to change both the strength and the elastic constants. Kachanov and associates have made calculations of the effect of microcracking on these two quantities and have found that whereas microcracking always produces a reduction of the stiffness (elastic property), the change in the stress intensity factor and therefore the change in the stress at the macrocrack tip depends on the arrangement of the microcracks in the vicinity of the macrocrack tip (refs 7, 9, 40, and 41). Amplification or shielding may occur, i.e., the stress at the macrocrack tip may be increased or decreased relative to the applied stress because of the presence of microcracks (refs 7, 40, and 41). For a given applied stress, the local stress may then be increased or decreased, and the stress for failure (e.g., fracture) can then be decreased or increased. The physical reason for the different effects of microcracking on the stiffness and the failure stress is that the stiffness is a volume average quantity while the failure stress is determined by conditions in the vicinity of the macrocrack tip (ref 9). However, in any finite sample many macrocracks

with associated microcracking will exist. Therefore, crack propagation and failure will tend to occur at those macrocracks where microcracking causes an amplification of the applied stress. A decrease in the applied stress for failure should be expected. The failure stress and the stiffness change then in the same direction with microcracking.

In contrast to the results of Kachanov and associates, Hutchinson has reported calculations which predict a decrease in the elastic modulus but also predict shielding and therefore an increase in the failure stress with microcracking (ref 42). Evans and Faber have also developed a model which predicts toughening and therefore an increase in the failure stress due to microcracking (ref 43). These workers cite experimental evidence to support their models. No attempt will be made here to evaluate these somewhat conflicting results. There is general agreement that microcracking results in a decrease in the elastic modulus, but there is no agreement on the prediction of the effects of microcracking on the failure strength. Further experimental results guided by theoretical work may be necessary to resolve this matter.

Because there is not an established relationship between microcracking and the fracture strength and the modulus, it is not possible to relate the observed relationship between the fracture strength and the modulus to microcracking. The reasons why microcracking might be different for the casts of Comp B, Comp B M1, and Comp B M2 are also not clear. Since the average moduli for Comp B M1 and Comp B M2 are larger than the modulus for Comp B, it is necessary to conclude that microcracking is greater in Comp B if, in fact, the differences are due to microcracking. Comp B M1 was made without wax and with recrystallized TNT. Comp B without wax tends to be more brittle and possibly more prone to microcracking than Comp B with wax. In addition, purification of TNT tends to make it brittle and so possibly more prone to microcracking (ref 36). If recrystallization of TNT produced purification, this could result in increased microcracking. Therefore, Comp B M1 might have increased microcracking and possibly a higher compressive strength but a lower modulus than Comp B and Comp B M2. The expected modulus change is then in the wrong direction to agree with the observations (table 4). Moreover, this approach does not give a rationale as to why Comp B M2 has a higher compressive strength than Comp B. Because solidification takes place more rapidly at the bottom of the cast, more microcracking might occur in this region and produce a gradient of microcracking with position in the cast. However, this argument leads to a lower modulus in the bottom of the cast in disagreement with observations. This approach also does not give a rationale for the lack of gradients in Comp B and TNT. For all of these reasons it is concluded that microcracking is most probably not responsible for the observed relationships between the compressive strengths, the moduli, and position in the cast for the four materials under discussion. Microcracking may, however, be responsible for a large part of the scatter in the data.

In summary, the relationship between the compressive fracture strength and the moduli for the three forms of Comp B can be attributed to differences in porosity. The relative differences in porosities of the three forms of Comp B are consistent with the differences in processing conditions used in preparing the casts from which the samples were taken. The changes in compressive fracture strength and modulus with position in the cast may also be due to porosity changes. The latter are consistent with the expected changes in porosity. While microcracking as a cause of the observed changes in fracture strength and modulus cannot be ruled out, the available results suggest that it is not the primary cause. The results also suggest that porosity may be a primary reason for the differences between the fracture strength and the modulus of TNT and the values for the three forms of Comp B. However, other considerations suggest that this is most probably not the case. Based on the porosity interpretation, the compressive fracture strength and the modulus of Comp B may be significantly increased by reducing the porosity.

Triaxial Results and Yield

The triaxial data and yield strength results are not nearly as extensive as the uniaxial data and compressive fracture strength results. Thus, the discussion of the triaxial results is more tentative and briefer than the discussion of the uniaxial results. While triaxial data are available for Comp B and TNT as a function of position in the cast, similar data are available for Comp B M1 only for the bottom portion of the cast and is not available as a function of position for Comp B M2. All triaxial data for Comp B M2 are for samples taken from the bottom section of the cast. The following is concerned largely with the differences in the yield strengths of Comp B, Comp B M1, and Comp B M2. The differences between Comp B and TNT have been discussed previously (ref 2). Factors which must be considered include porosity, cracking, and other inhomogeneities such as RDX particles which can give rise to impediments to dislocation motion. The experimental relationship between the yield strength, Y, and the modulus, E, (fig. 14) indicates the Y and E are approximately the same function of one or more variables so that the ratio Y/E is constant as the variables are changed as is the case with the ratio σ_m/E.

The general approach based on the idea that the local stress is increased relative to the applied stress when porosity is present because of a decrease of the load bearing area and/or stress concentrations is also applicable to yield strength considerations. Therefore, the yield strength Y can be given as a first approximation as a function of porosity by an expression of the same form as equation 5, i.e.,

$$Y = Y_o e^{-b_Y P} \tag{10}$$

and the relationship between Y and E is

$$Y = E_Y Y_o / E_{oY} e^{-(b_Y - b_{EY})P} \tag{11}$$

using equation 6 and 10. The subscript Y for E_Y, E_{oY}, and b_{EY} is used to indicate the modulus as determined by triaxial measurements. The quadratic term in equation 6 has been omitted in obtaining equation 11. The exponential term of equation 11 can be expanded to give

$$Y = E_Y Y_o / E_{oY}[1 - (b_Y - b_{EY})P] \tag{12}$$

when

$$(b_Y - b_{EY})P << 1 \tag{13}$$

as for equation 8.

The data for Comp B, Comp B M1, and Comp B M2 as plotted in figure 14 suggest an approximately linear relationship between Y and E as predicted by equation 12 when equation 13 is satisfied. The large scatter prohibits a more detailed analysis of the data of figure 14. The results in this figure suggest, however, that the relative yield strengths of the three forms of Comp B are determined by porosities. The yield strength results can be interpreted in the same way as the compressive fracture strength results.

As noted, triaxial data are available for Comp B M1 as a function of position in the cast only for the bottom portion of the cast and is not available for Comp B M2. Within this limitation, the available data for Comp B M1 indicate that the yield strength decreases as the distance from the top of the cast increases although the moduli of the same samples increase slightly as this distance increases (fig. 6). For these limited data for Comp B M1 as a function of position, the yield strength does not change in the same direction as the compressive fracture strength and the modulus with position. However, for the data of Comp B M2, which is for samples taken from one position near the bottom of the cast, the yield strength and the modulus change in the same direction from sample to sample. Because of these limited results, it is necessary to conclude that the relationship between yield strength, modulus, and position in the cast is not as consistent as is the relationship between compressive fracture strength, modulus, and position in the cast.

As already pointed out, densities and therefore porosities are not available for most of the samples of Comp B M1 and Comp B M2. However, they are available for some of the samples from the bottom portions of the casts of these two materials which were used for the triaxial studies. The logarithms of the yield strengths and the triaxial moduli are plotted versus the average porosities for Comp B, Comp B M1, and Comp B M2 in figures 17 and 18. Straight lines were fitted by a least-squares technique to the

points of these figures (without TNT) as predicted by equation 6 (with c = 0) and equation 10 to give b_{EY} = 29, E_{oY} = 1.1 x 10^6 psi, b_Y = 46, and Y_o = 2.0 by 10^5 psi. b_{EY} and E_{oY} are less than b_E and E_o obtained from the uniaxial data but the value of b_Y is the same as the value of b_σ = 46 also obtained from the uniaxial data. In addition, the ratio Y_o/E_{oY} obtained from the fits in lnY and lnE_Y versus P is 1.9 x 10^{-2}. This value is reasonably close to the value of 1.53 x 10^2 obtained from the data of figure 14. All of this supports the hypothesis that the relative yield strengths of these three materials are determined by differences in porosity. The discussion of this paragraph also suggests that the porosities as calculated from the densities are accurate although all of the arguments presented in the section dealing with the compressive strength and porosity still apply. The similarity of b_σ and b_Y supports the contention that the local stress which is responsible for both crack growth leading to fracture and dislocation motion leading to yield is increased relative to the applied stress because of porosity. The porosities obtained from the available densities are approximately 2% or less. The value of Y_o indicates that much larger yield strengths may be obtained by reducing the porosity.

An inspection of figure 14 reveals that the straight line fitted to the points for the Comp B's does not pass through the points for TNT. However, straight lines were fitted to the points of figure 17 and 18 including the points for TNT. In this case, b_Y, Y_o, b_{EY}, and E_{oY} are not significantly changed from the values found without the TNT points, suggesting that the relative yield strengths of TNT and the Comp B's are determined primarily by porosity.

However, a different explanation was given previously for the differences in the yield strengths of TNT and Comp B based on the temperature and strain rate dependencies. The yield strength of Comp B has been interpreted in terms of long range internal stress fields and barriers to dislocation motion which are overcome by thermal activation. In contrast, the yield strength of TNT has been interpreted only in terms of long range internal stress fields. The yield strengths of the two materials are close at temperatures slightly below the melting temperature of TNT and are thought to be primarily determined by the long range internal stress fields in both materials. However, at 35°C the yield strength of Comp B is increased significantly over the value at elevated temperatures due to the barriers to dislocation motion (and thermal activation) while the yield strength of TNT is not increased significantly for this same change in temperature. Therefore, the difference in the yield strengths of the two materials at 35°C has been attributed to the presence of barriers to dislocation motion in Comp B which are not present or active in TNT. It was further suggested that the barriers to dislocation motion in Comp B may be associated with RDX in solution in the TNT of

Comp B if yield occurs primarily in the TNT of Comp B. It therefore seems necessary to conclude at this time that if the primary reason for the difference in the yield strengths of TNT and Comp B at 35°C are as given previously and sketched here, then porosity cannot also play a major role in this difference. The long range internal stress fields and the barriers to dislocation motion could be associated with porosity, but effects of this type on the yield strength would be in addition to the changes in local stresses due to porosity. To determine if the primary difference in the yield strengths of Comp B and TNT is due to barriers to dislocation motion, porosity or both requires more extensive yield strength data as a function of temperature, strain rate, and porosity.

The yield strength may also be influenced by the presence of cracks and the reduction of the yield strength and the modulus by a particular symmetry of cracks has been calculated (ref 11). Cracks are taken as all aligned in one direction and all cracks have the same lengths, widths, and separations. With loading perpendicular to this direction, there are significant reductions of the modulus and the yield strength which increase with increases in the crack lengths. The predicted (and observed) relationship between the yield strength and the modulus with increasing crack length is not linear but could easily be used to describe the data of figure 14 because of the scatter of the data points. The calculated yield strength is obtained by elastic strain energy considerations for the material containing cracks. However, the reduction of the load bearing area is explicitly taken into account in terms of a damage sensor. Therefore, the model includes the effects of porosity as represented by the cracks. While the model is highly idealized and most probably does not represent the conditions in the samples used in this study, it suggests that the observed relationship between Y and E may be obtained by a consideration of the effect of cracks by the general approach used by Litewka.

In summary, the limited triaxial data which indicate a relationship between the yield strength and the modulus for the Comp B's can be interpreted on the basis of porosity being the primary cause of this relationship and the differences in these quantities from sample to sample and from one form of Comp B to another. The idealized crack model used by Litewka also predicts a relationship between yield strength and modulus which is compatible with the available data. While the results suggest that porosity could be the primary cause of the differences in the yield strengths and moduli of TNT and the values for the Comp B's, other considerations indicate that this may not be the case. Additional data are required to further resolve this matter.

SUMMARY AND CONCLUSIONS

Three composites of RDX and TNT and the matrix material (TNT) have been studied in uniaxial and triaxial (radially confined) compression at temperatures of 23°C and 35°C, respectively. Two of the composites also contained wax. All four materials were cast but with somewhat different casting (processing) conditions. The average

compressive fracture strength, the average yield strength, and the average value of Young's modulus differ for all four materials. For two of the composites, the compressive fracture strength and Young's modulus increased with distance from the top of the cast. In contrast, these properties are independent of this distance for the other composite (Composition B) and for the matrix material (TNT). Linear relationships were found between the compressive fracture strength and the modulus and between the yield strength and the modulus. These relationships can be attributed to exponential dependencies of the fracture strength, the yield strength, and the modulus on porosity. Porosity data obtained from limited density measurements tend to confirm this suggestion and the differences in the porosities of the three composites are consistent with the differences in processing conditions. The results further indicate that significant increases in the compressive fracture strength, the yield strength, and Young's modulus may be attained by a reduction of the porosity. Microcracking may also play a role in the differences in the observed properties. The results also indicate that changes in RDX particle size and omission of wax do not significantly alter the observed mechanical properties of the composite (Composition B). However, the results are somewhat incomplete so that the interpretation must be regarded as tentative. Additional mechanical measurements are necessary in all areas to give statistical weight to the results and porosity determinations are essential.

Table 1. Composition

	COMP B	COMP B M1	COMP B M2	TNT
RDX	59.5% Class 1 (course)	60.0% Class 1 (course)	59.4% Class 7 (fine)	
TNT	39.5% Military Grade	40.0% Military Grade Recrystallized	39.6% Military Grade	100% Military Grade
WAX	1.0%	None	1.0% Petrolite (ES-670)	
HMX	Unknown	7.4% of RDX	9.3% of RDX	

Table 2. Material characterization

RDX Particle Size Distribution

SIEVE NUMBER	SIEVE OPENING (MM)	GRADE 1 (COURSE) % PASSING	GRADE 7 (FINE) % PASSING
20	0.84	100%	100%
50	0.30	93.6%	97.0%
100	0.149	34.4%	66.8%
200	0.074	11.0%	56.5%
325	0.044	0	

TNT

TNT TYPE	MILITARY GRADE	MILITARY GRADE RECRYSTALLIZED
TNT MELTING TEMPERATURE	82.5°C	82.5°C

Table 3. Processing conditions

	MOLD AND RISER PRE-HEATED	VACUUM TO MELT	POUR TEMP	FILLED MOLD VIBRATED	STEAM HEATED PROBE IN TOP OF MOLD	FILLED MOLD WRAPPED IN INSULATION
COMP B	YES	NO	82°C	NO	YES	YES
COMP B M1	YES	12 MIN	80°C	NO	YES	YES
COMP B M2	YES	12 MIN	92°C	12 SEC	YES	YES
TNT	YES	NO	76°C	NO	YES	YES

Table 4. Uniaxial results T = 23°C

	COMP B	COMP B M1	COMP B M2	TNT
σ_m COMPRESSIVE STRENGTH (PSI)	3,260 ±150	4,020 (2,700 to 5,050)	4,240 (3,500 4,900)	1,850 ±180
E YOUNG'S MODULUS (X10^6 PSI)	0.60 ±0.02	0.81 (0.61 to 0.88)	0.79 (0.59 to 0.92)	0.45 ±0.07

Table 5. Triaxial results T = 35°C

	COMP B	COMP B M1	COMP B M2	TNT
Y YIELD STRENGTH (PSI)	7,420 ±1050	11,300 (8,400 to 13,500)	11,030 (7,500 to 14,000)	3,350 ±290
E YOUNG'S MODULUS (X10^6 PSI)	0.54 ±0.07	0.74 (0.69 to 0.80)	0.65 (0.47 to 0.85)	0.37 ±0.06
ν POISSON'S RATIO	0.36 ±0.02	0.30 ±0.03	0.31 ±0.04	0.39 ±0.02

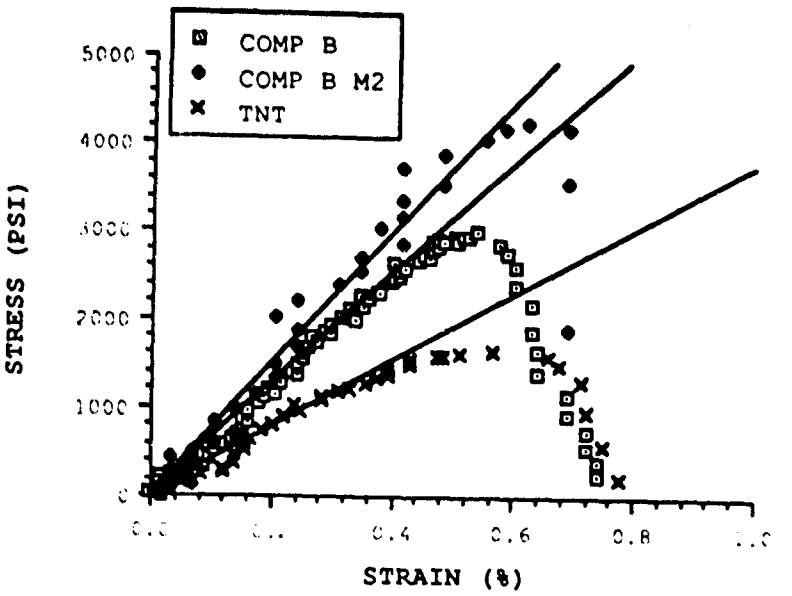

Figure 1. Uniaxial compressive stress versus strain for two composites and the matrix material

NOTE: The modulus has been taken from the straight lines through the initial data points in each case.

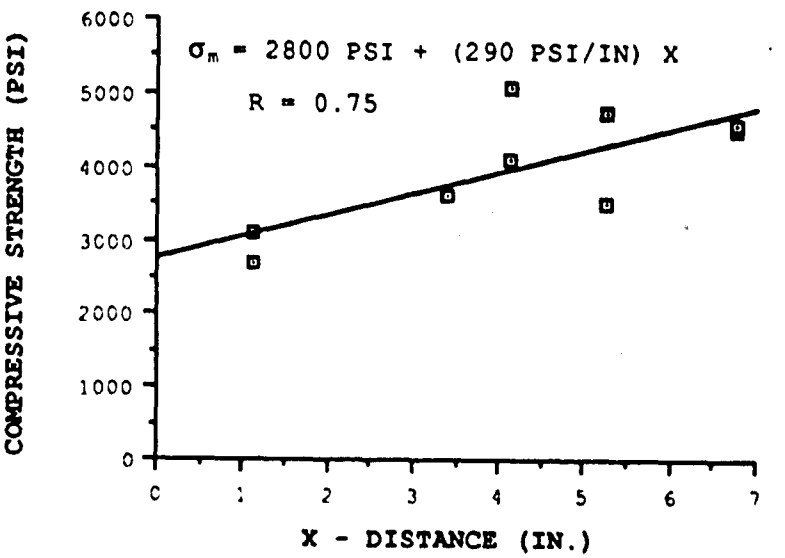

Figure 2. Compressive strength versus distance from the top of the cast for Comp B M1

NOTE: The line is a least-square fit of a straight line to the data points. R is the correlation coefficient (ref 14).

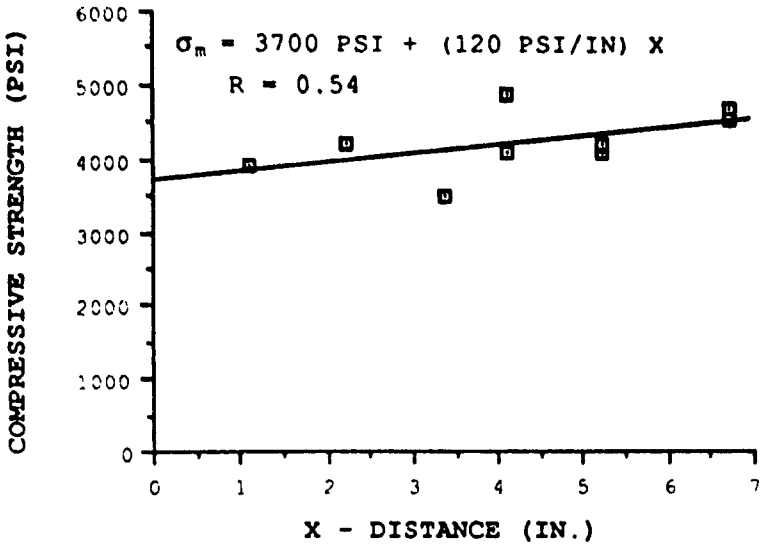

Figure 3. Compressive strength versus distance from the top of the cast for Comp B M2

NOTE: The line is a least-square fit of a straight line to the data points. R is the correlation coefficient (ref 14).

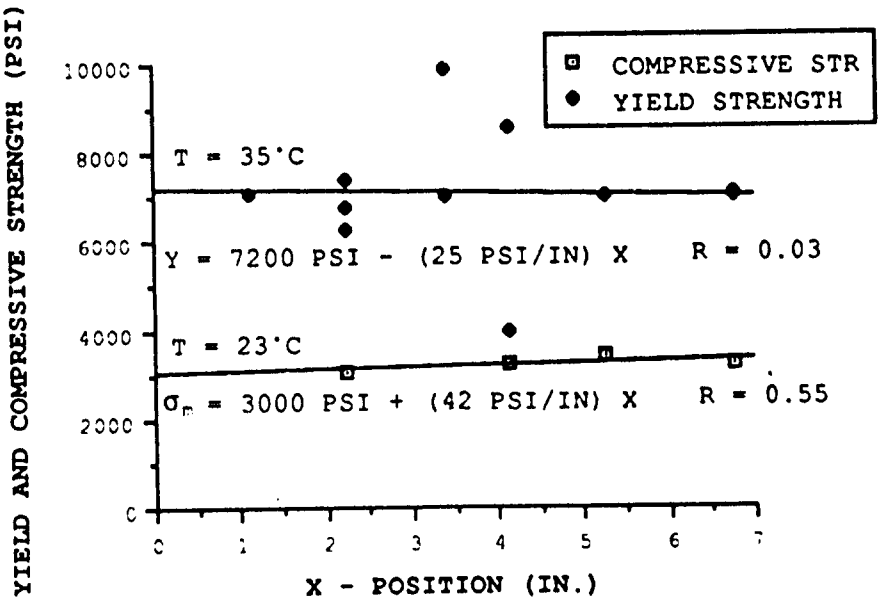

Figure 4. Compressive strength and yield strength versus distance from the top of the cast for Comp B

NOTE: The lines are least-square fits of straight lines to the data points. R is the correlation coefficient (ref 14).

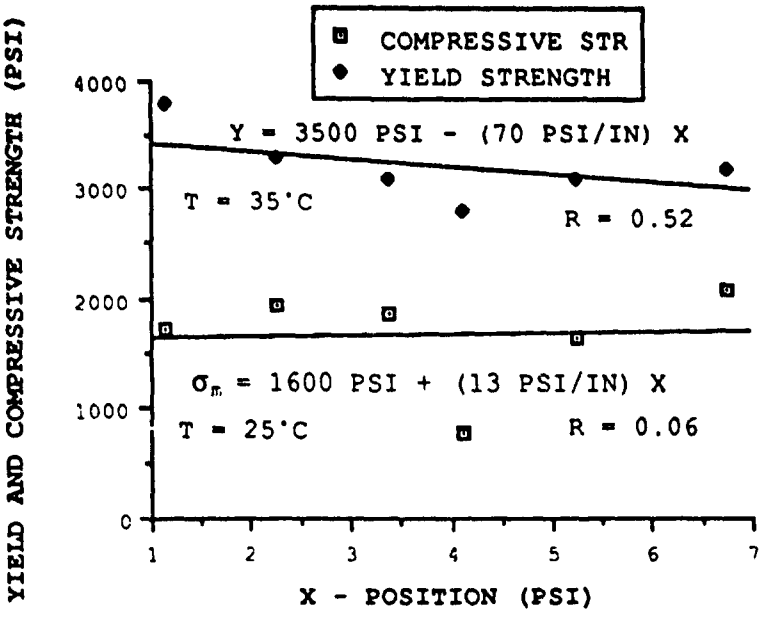

Figure 5. Compressive strength and yield strength versus distance from the top of the cast for TNT

NOTE: The lines are least-square fits of straight lines to the data points. R is the correlation coefficient (ref 14).

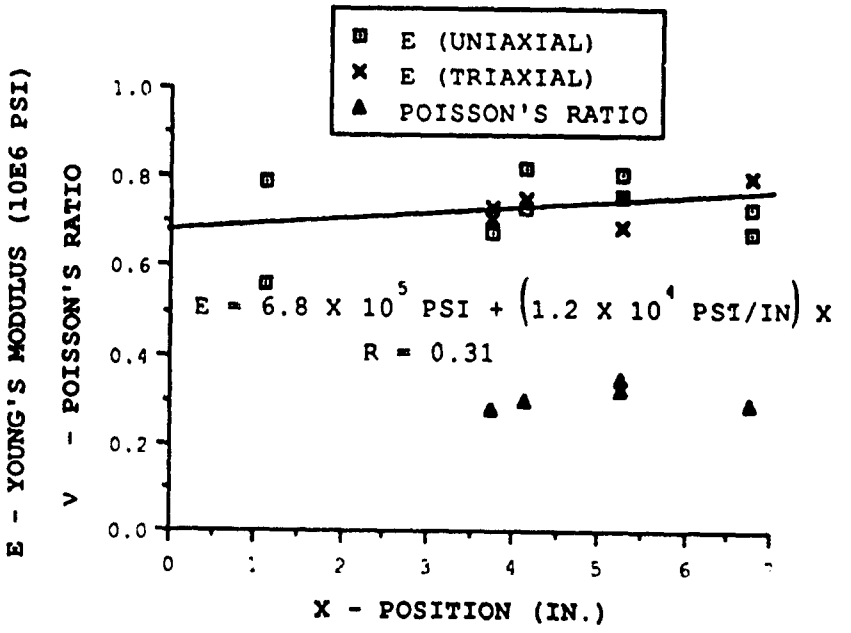

Figure 6. Young's modulus and Poisson's ratio versus distance from the top of the cast for Comp B M1

NOTE: The line is a least-square fit of a straight line to the data points. R is the correlation coefficient (ref 14).

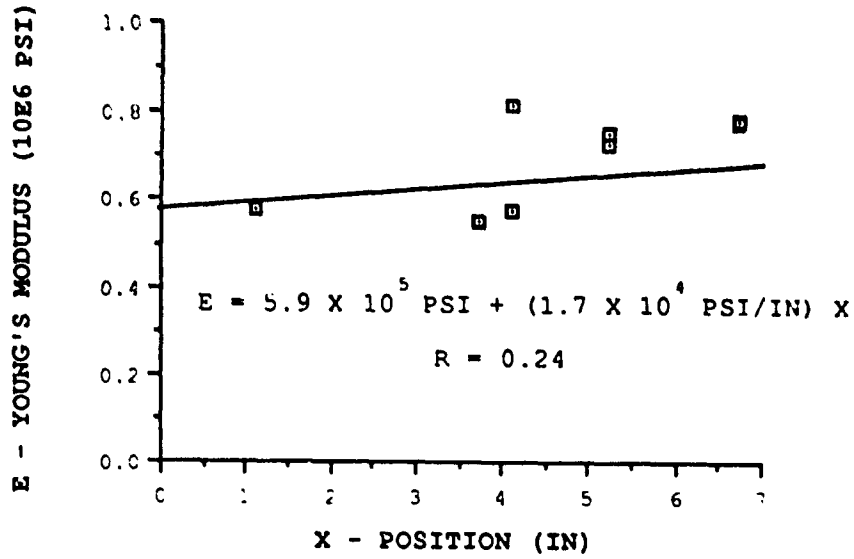

Figure 7. Young's modulus versus distance from the top of the cast for Comp B M2

NOTE: The line is a least-square fit of a straight line to the data points. R is the correlation coefficient (ref 14).

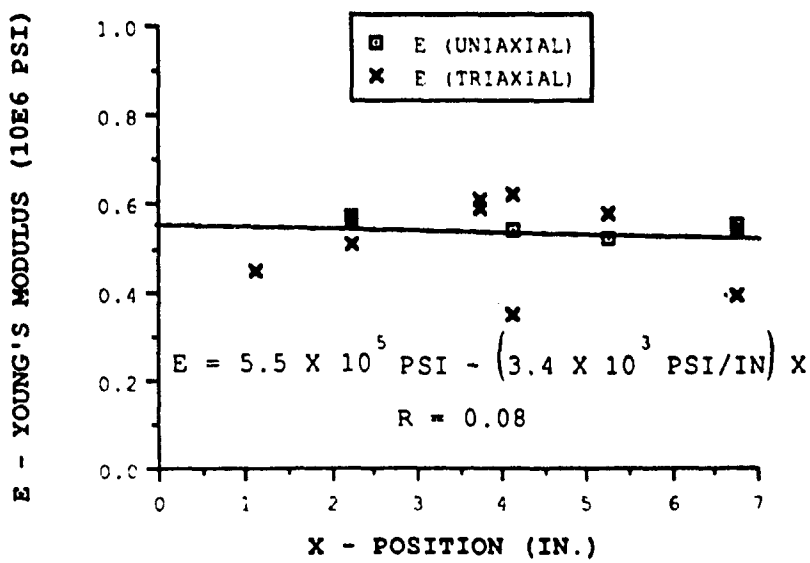

Figure 8. Young's modulus versus distance from the top of the cast for Comp B

NOTE: The line is a least-square fit of a straight line to the data points. R is the correlation coefficient (ref 14).

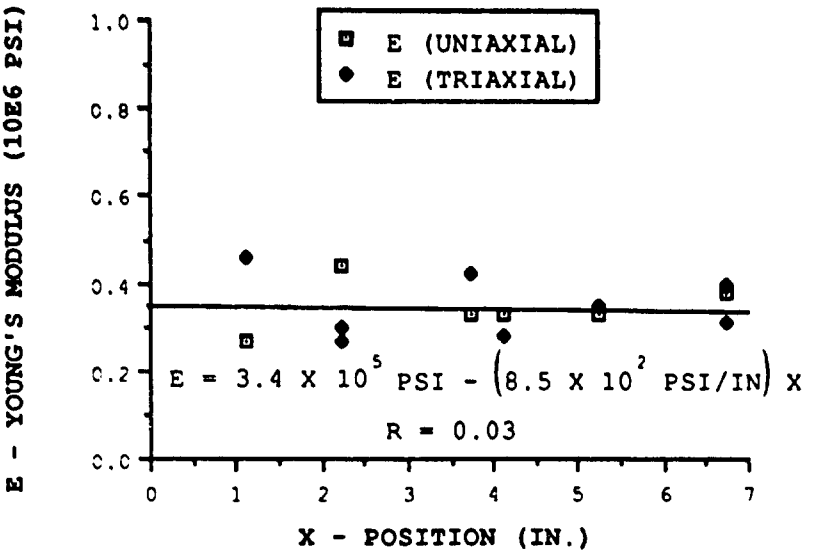

Figure 9. Young's modulus versus distance from the top of the cast for TNT

NOTE: The line is a least-square fit of a straight line to the data points. R is the correlation coefficient (ref 14).

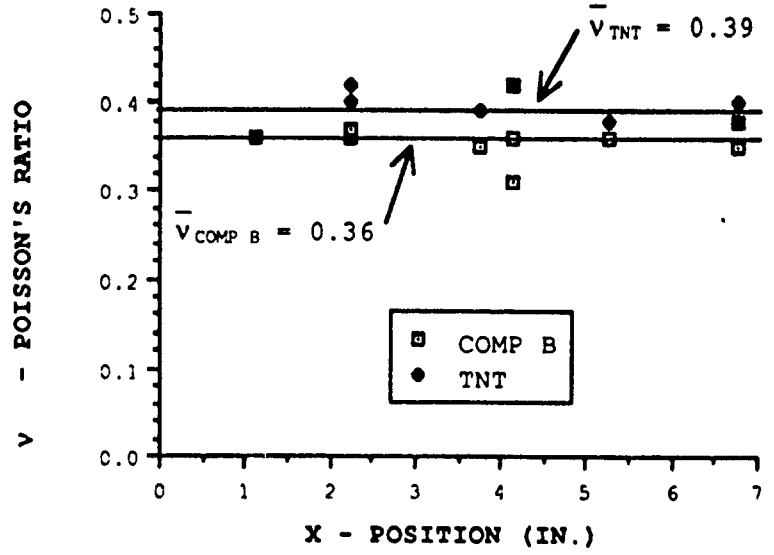

Figure 10. Poisson's ratio versus distance from the top of the cast for Comp B and TNT

NOTE: The straight lines are least-square fits of straight lines to the data points. R is the correlation coefficient (ref 14).

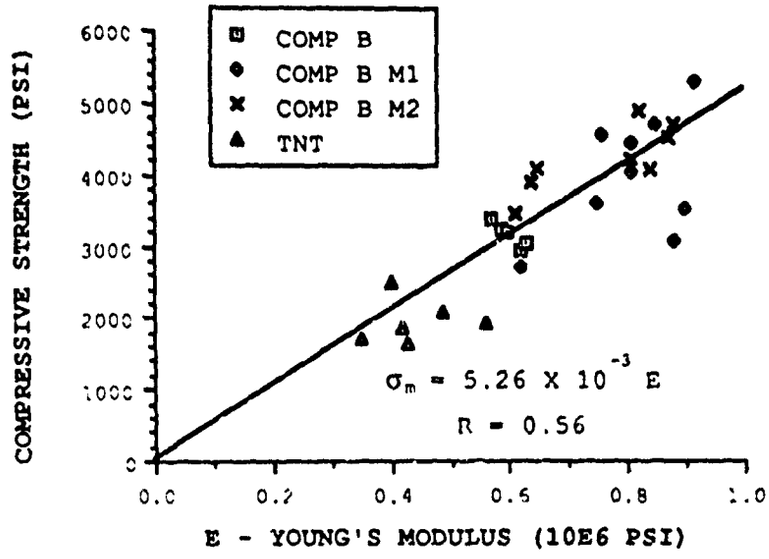

Figure 11. Compressive strength versus Young's modulus for all materials

NOTE: The line is a least-square fit of a straight line through the origin to the data points for the three composites only. R is the correlation coefficient (ref 14).

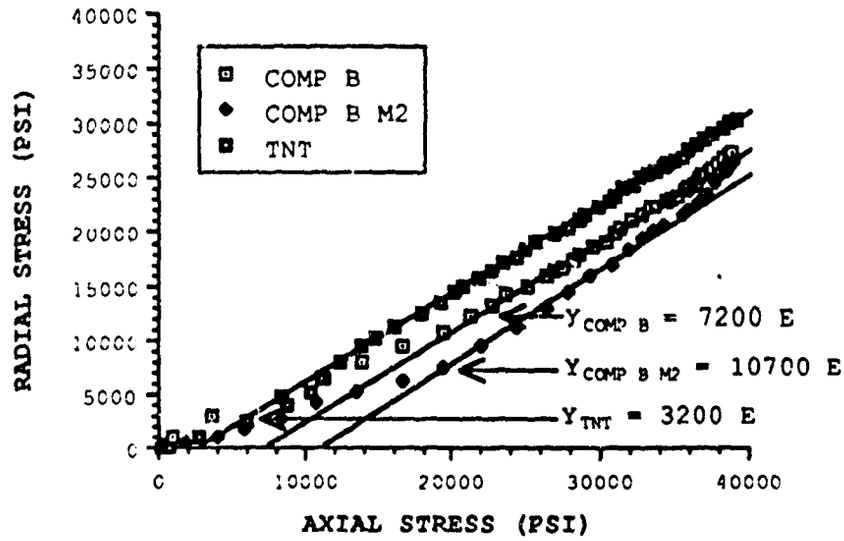

Figure 12. Radial stress versus axial stress for the (confined cylinder) triaxial loading conditions for two of the composites and the matrix material

NOTE: The yield strengths were determined from the axial stress intercepts of straight lines through the data points for stresses above yield.

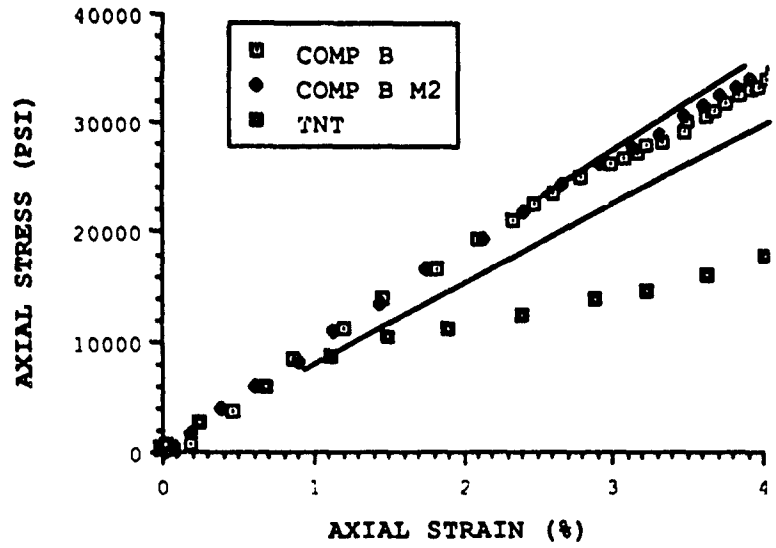

Figure 13. Axial stress versus axial strain for the (confined cylinder) triaxial loading conditions for two of the composites and the matrix material

NOTE: The straight lines indicate the slopes before yield for the Comp Bs and TNT respectively. Young's modulus is obtained from these slopes.

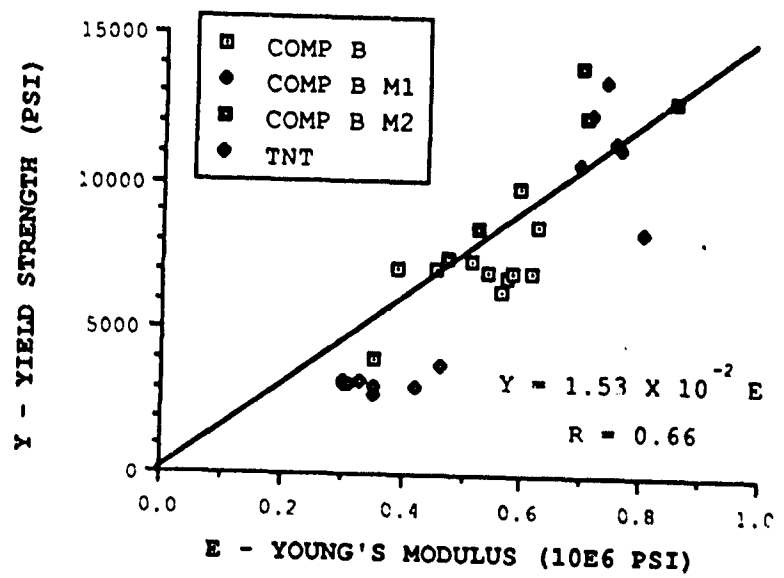

Figure 14. Yield strength versus Young's modulus for all four materials

NOTE: The line is a least-square fit of a straight line through the origin to the data points for the three composites only. R is the correlation coefficient (ref 14).

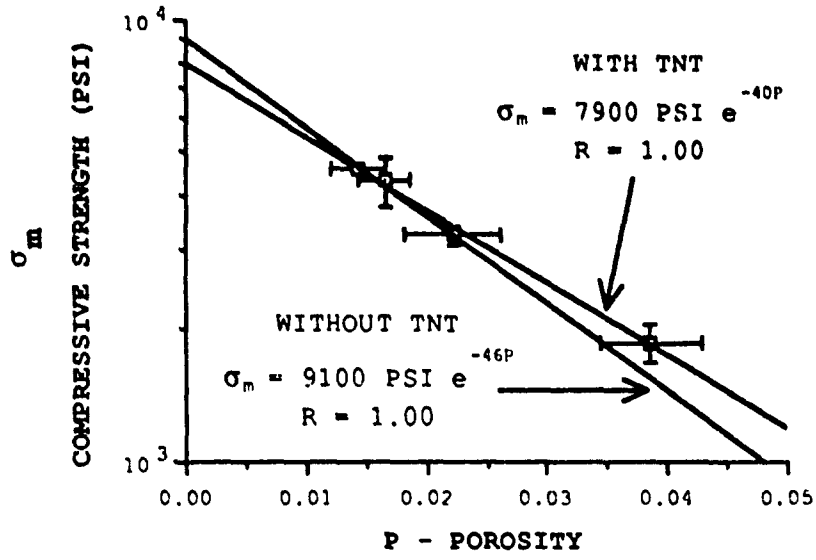

Figure 15. Compressive strength versus porosity

NOTE: The lines are least-square fits of straight lines to the data points with and without TNT (largest porosity). R is the correlation coefficient (ref 14).

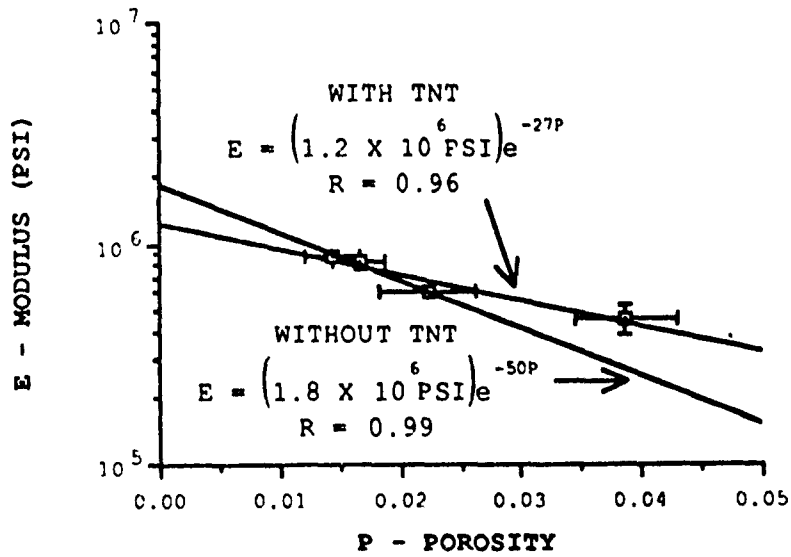

Figure 16. Young's modulus from uniaxial data versus porosity (see test)

NOTE: The lines are least-square fits of straight lines to the data points with and without TNT (largest porosity). R is the correlation coefficient (ref 14).

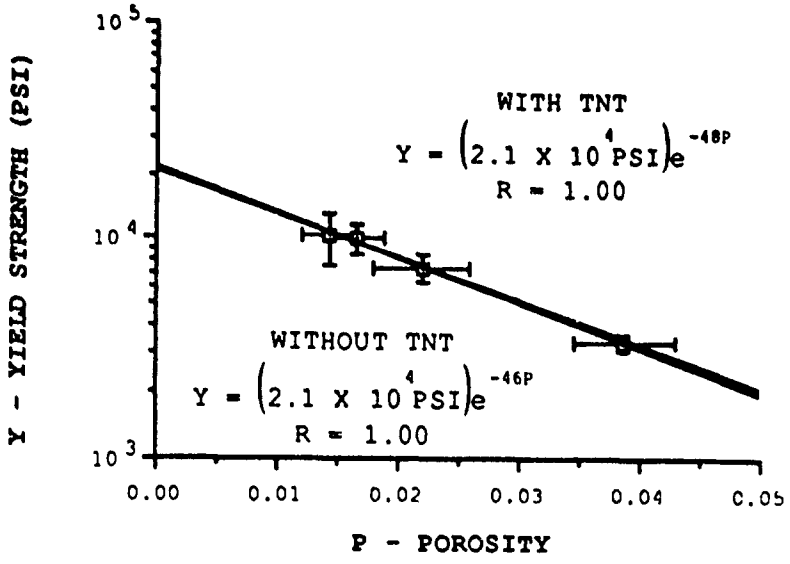

Figure 17. Yield strength versus porosity

NOTE: The lines are least-square fits of straight lines to the data points with and without TNT (largest porosity). R is the correlation coefficient (ref 14).

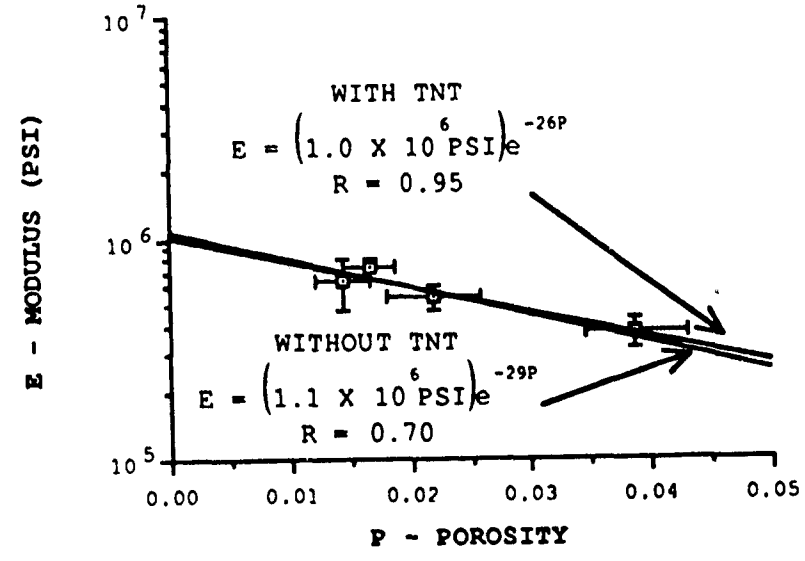

Figure 18. Young's strength versus porosity

NOTE: The lines are least-square fits of straight lines to the data points with and without TNT (largest porosity). R is the correlation coefficient (ref 14).

REFERENCES

1. Pinto, J.; Wiegand, D. A.; and Nicolaides, S., J. Energetic Materials, 9, 19 (1991).

2. Pinto, J. and Weigand, D. A., J. Energetic Materials, 9, 205 (1991).

3. Pinto, J.; Nicolaides, S.; and Wiegand, D. A., "Dynamic and Quasi Static Mechanical Properties of Comp B and TNT", Technical Report ARAED-TR-85004, Picatinny Arsenal, NJ, 1985.

4. Starkenberg, J. J.; MaFadden, D. L.; and Lyman, O. R., Technical Report BRL-TR-2714, 1986.

5. Belanger, C., Ninth Symposium (International) on Detonation, Portland, OR, 1989.

6. Schafer, S., DEA 1218 Meeting, Test Center, Meppen, FRG, June 1986.

7. Kachanov, M. and Montagut, E., Engr. Fracture Mech. 25, 625 (1986).

8. Knudsen, F. P., J. Am. Ceramic Soc. 42, 376 (1959).

9 Montagut, E. and Kachanov, M., Inter. J. Fracture 37, R55 (1988).

10. Wang, J. C., J. Mat. Sci. 19, 801, 809, (1984).

11. Litewka, A., Engr. Fracture Mech. 25, 637 (1986).

12. Wiegand, D. A. and Pinto, J., Materials Research Society Symposium Proceedings: Mechanical Properties of Porous and Cellular Materials, in press.

13. Wiegand, D. A. and Pinto, J., to be published.

14. Papoulis, A., "Probability, Random Variables, and Stochastic Processes," McGraw-Hill, NY, Second Edition, P 150, 1984.

15. Georgevich, D., private communication.

16 See for example Rice, R. W., Proc. Britt. Cer. Soc. 21, 205 (1972).

17. See for example: Coble, R. L. and Parikh, N. M., "Fracture," Vol. VII, p 269, ed. Liebowitz, H., Academic Press, New York (1972).

18. Ibid. p 284.

19. Duke, J. R. C., "Crystallography of TNT," Explosives Research and Development Establishment, Waltham Abbey (1974).

20. Choi, C. S., Acta. Crysta. B28, 2857 (1972).

21. Heberlein, D. C., U.S. Army Mobility Equipment Research and Development Command, Fort Belvoir, VA, Report 2202, (1976) and J. Chem. Physics, 61, 2346 (1974).

22. Lanzerotti, M. Y.; Pinto, J.; and Wolfe, A., Ninth Symposium (International) on Detonation, August 1989 (to be published).

23. Morrow, S., Private Communication.

24. Smith, D. L. and Thorpe, B. W., J. Mater. Sci. Lett. 8, 757 (1973).

25. Hagan, J. T. and Chaudhri, M. M., J. Mater. Sci. Lett. 12, 1055 (1977).

26. Rice, R. W., "Treatise on Material Science and Technology," Vol. 11, ed. Mac-Crone, R. K., Academic Press, New York, 1977.

27. Costain, T. and Motto, R., Technical Report 4587, Picatinny Arsenal, NJ 1973.

28. MIL-R-398C.

29. Lanzerotti, M.Y., Private Communication.

30. Nicolson, P. S., High Temp. Sci., 13, 279 (1980).

31. Alford, N. McN., Matl. Sci. and Engr. 56, 279 (1982).

32. Bentur, A. and Mindess, S., Cement and Concrete Res. 16, 59 (1986).

33. Zielinski, A. J. and Reinhardt, H. W., Cement and Concrete Res. 12, 309 (1982).

34. Zeigler, G. Unpublished Results.

35. Croom, R.; Taschler, A.; Ark, F.; and Chen, T. H., "Technology of Polymer Compounds and Energetic Materials," 21st International Conference of ICT 1990, Karlsruhe, Germany, to be published.

36. Joyce, M., Private Communication.

37. See Reference 26, pp 266-282.

38. See Reference 26, p 342.

39. See Reference 26, p 220.

40. Kachanov, M. and Laures, J. P., Inter J Fracture 37, R63 (1988).

41. Kachanov, M., Inter J Solid Structures 23, 23 (1987).

42. Hutshinson, J. W., Acta Metall 35, 1605 (1987).

43. Evans, A. G. and Faber, K. T., J Am Ceramic Soc 67, 255 (1984).

DISTRIBUTION LIST

Commander
Armament Research, Development and Engineering Center
U.S. Army Armament, Munitions and Chemical Command
ATTN: SMCAR-IMI-I (5)
SMCAR-AEE-W, M. Kirschenbaum
N. Slagg
SMCAR-AEE-WW, B. Fishburn
J. Pinto
M. Mezger
Y. Lanzerotti
D. Wiegand (15)
SMCAR-AES, S. Kaplowitz
SMCAR-AEE
SMCAR-AEE-B, D. Downs
S. B. Berstein
E. Costa
SMCAR-CCH-V, F. Hildebrant
SMCAR-AEE, J. Lannon
SMCAR-AEE-BR, T. Beardell
SMCAR-AET-M, A. Rupel
SMCAR-AET-M, S. Cytron (2)
Picatinny Arsenal, NJ 07806-5000

Commander
U.S. Army Armament, Munitions and Chemical Command
ATTN: AMSMC-GCL (D)
AMSMC-PBM, A. E. Siklosi
D. Fair
AMSMC-QAR-R, L. Manole
E. Bixon
Picatinny Arsenal, NJ 07806-5000

Administrator
Defense Technical Information Center
ATTN Accessions Division (12)
Cameron Station
Alexandria, VA 22304-6145

Director
U.S. Army Materiel Systems Analysis Activity
ATTN: AMXSY-MP
Aberdeen Proving Ground, MD 21005-5066

Commander
Chemical Research, Development and Engineering Center
U.S. Army Armament, Munitions and Chemical Command
ATTN: SMCCR-MSI
SMCCR-SPS-IL
Aberdeen Proving Ground, MD 21010-5423

Commander
Chemical Research, Development and Engineering Center
U.S. Army Armament, Munitions and Chemical Command
ATTN: SMCCR-RSP-A
Aberdeen Proving Ground, MD 21010-5423

Director
Ballistic Research Laboratory
ATTN: AMXBR-OD-ST
AMXBR-BLT, R. Frey
P. Howe
AMXBR-BLC, J. Starkenberg
AMXBR-TBT, R. Lieb
J. Rocchio
Aberdeen Proving Ground, MD 21005-5066

Chief
Benet Weapons Laboratory, CCAC
Armament Research, Development and Engineering Center
U.S. Army Armament, Munitions and Chemical Command
ATTN: SMCAR-CCB-TL
SMCAR-LCB-RA, J. Vasilakis
Watervliet, NY 12189-5000

Commander
U.S. Army Armament, Munitions and Chemical Command
ATTN: AMSMC-IMF-L
AMSMC-ESM, W. D. Fortune
AMSMC-IRD, G. H. Cowan
Rock Island, IL 61299-6000

Director
U.S. Army TRADOC Systems Analysis Activity
ATTN: ATAA-SL
White Sands Missile Range, NM 88002

Office of the Secretary of Defense
OUSD(A)
Director, Live Firing Testing
ATTN: James F. O'Bryon
Washington, DC 20301-3110

Director
U.S. Army Aviation Research and Technology Activity
Ames Research Center
Moffett Field, CA 94035-1099

HQDR (SARD-TR)
Washington, DC 20310-0001

Commander
U.S. Army Materiel Command
ATTN: AMCDRA-ST
AMCPM-GCM-WF
AMCDE-DW
5001 Eisenhower Avenue
Alexandria, VA 22333-0001

Commander
U.S. Army Laboratory Command
ATTN: AMSLC-DL
2800 Powder Mill Road
Adelphi, MD 20783-1145

Commander
U.S. Army Missile Command
ATTN: AMSMI-RD-CS-R (DOC)
Redstone Arsenal, AL 35898-5010

Commander
U.S. Army Tank-Automotive Command
ATTN: AMSTA-TSL (Technical Library)
Warren, MI 48397-5000

Commandant
U.S. Army Infantry School
ATTN: ATSC-CD-CSO-OR
Fort Benning, GA 31905-5660

Air Force Armament Laboratory
ATTN: AFATL-DLODL
AFATL/DOIL
Eglin Air Force Base, FL 32542-5000

Director
USAMSAA
ATTN: AMXSY-D
AMXSY-MP, H. Cohen
Aberdeen Proving Ground, MD 21010-5423

U.S. Army Ballistic Missile Defense Systems Command
Advanced Technology Center
ATTN: D. Sayles
P.0. Box 1500
Huntsville, AL 35807-3801

Commander
Naval Surface Warfare Center
ATTN: R10C, L. Roslund
R13, J. Short
R. Bernecker
F. Forbes
R10B, M. Stosz
Silver Spring, MD 20903-5000

Air Force Rocket Propulsion Laboratory
ATTN: AFRPL MKPA, R. Geisler
Edwards AFB, CA 93523-5000

Commander
U.S. Army Aviation Systems Command
ATTN: AMSAV-DACL
4300 Goodfellow Blvd
St. Louis, MO 63120-1798

Commander
U.S. Army Research Office
ATTN: Chemistry Division
P.O. Box 12211
Research Triangle Park, NC 27709-2211

Commander
Naval Weapons Center
ATTN: L. Smith
A. Amster
R. Reed, Jr.
China Lake, CA 93555

Southwest Research Institute
ATTN: M. Cowperthwaite
H. J. Grything
6220 Culebra Road
Postal Drawer 28510
San Antonio, TX 78284

New Mexico Institute of Mining and Technology
ATTN: TERA, T. Joyner
Campus Station
Socorro, NM 87801

Director
Lawrence Livermore National Labortory
ATTN: R. McGuire
K. Scribner
E. Lee
M. S. Costantino
L-324
M. Finger
P.O. Box 808
Livermore, CA 94550

Director
Los Alamos National Laboratory
ATTN: J960, J. Ramsay
P.O. Box 1663
Los Alamos, NM 87545

Director
Sandia National Laboratory
ATTN: J. Kennedy
Albuquerque, NM 87115

Honeywell, Inc.
ATTN: R. Tompkins
10400 Yellow Circle Drive
MN 38-3300
Minnetonka, MN 55343

Johns Hopkins University
Applied Physics Laboratory
Chemical Propulsion Information Agency
ATTN: John Hannum
Johns Hopkins Road
Laurel, MD 20707

Morton Thiokol Inc.
Louisiana Division
ATTN: Lee C. Estabrook
P.O. Box 30058
Shreveport, LA 71130

Commander
Naval Weapons Station
ATTN: L. Rothstein
Code 50 - NEDED
Yorkstown, VA 23491